J. Indian Inst. Sci., July–Aug. 1996, **76**, 437–463.

Materials response under static and dynamic high pressures*

R. CHIDAMBARAM
High Pressure Physics Division, Bhabha Atomic Research Centre (BARC), Bombay 400 085, India.

Received on April 30, 1996.

Abstract

Studies on equation of state and phase transitions at high pressures have significantly contributed to our basic understanding of condensed matter physics. High-pressure data on materials also find important applications in applied sciences. The developments in first principle theories and experimental techniques are listed. The similarities and differences in behaviour of materials under static and dynamic pressures are discussed. The article also describes the current interplay between theoretical and experimental high-pressure research with illustrations from our own studies and emphasis on future scope.

Keywords: Equation of state, phase transition, shock Hugoniot, diamond anvil cell.

1. Introduction

The use of pressure to alter the physical and chemical states of materials is as fundamental as varying the chemical composition or temperature. Volume reduction obtained in materials by current high-pressure techniques is an order of magnitude higher than the change brought about by temperature. This high compression is achieved using static and dynamic pressures. Static high-pressure techniques have evolved from the use of hardened steel anvils to the current novel diamond anvil cell device[1]. Diamond anvil cell technology has brought about a revolution in terms of the range of pressures achieved and in the wide variety of diagnostic techniques that can be employed because diamonds act as excellent windows through which the sample can be viewed[1–2]. It is possible to use a wide range of electromagnetic radiation to characterize the physical properties of samples *in situ* at high pressures. These newly acquired capabilities have enabled researchers to exploit fully the pressure variable. On the other hand, dynamic high pressures are generated by introducing a rapid impulse into a material through the detonation of a high explosive, with the impact of a high-speed projectile or by the absorption of an intense pulse of radiation[3]. High-speed optical and electronic methods are necessary to measure certain dynamic variables which determine density, pressure and energy. However, till recently, the diagnostic techniques used were mostly for carrying out measurements of continuum parameters. Unlike the static case, the *in-situ* probing of samples during the passage of shock wave is extremely difficult. Nevertheless, flash X-ray diffraction measurements by Johonson and Mitchell[4] followed by the work of Whit-

*Text of lecture delivered at the Annual Faculty Meeting of the Jawaharlal Nehru Centre for Advanced Scientific Research at Bangalore on November 11, 1995.

lock and Wark using laser-driven shocks has opened up the possibility of online examination of samples under shock. Currently, various laboratories are seriously engaged in developing techniques to generate time-resolved optical data[6] and to carry out X-ray diffraction measurements under shock conditions[5,7]. However, the development of these techniques to obtain reliable data still remains a tough task. The limited time scales, the need for uniaxial configuration and destructive nature of the experiments severely limit such measurements which are widely employed in static high-pressure experiments. In static high-pressure studies measurements are carried out along the isotherms with a combination of ultrahigh-pressure and laser-heating techniques. It is possible to obtain isotherms of several thousand degrees Celsius at different pressures in materials using the diamond anvil cell[8,9]. Such controlled high-pressure temperature conditions can be realised for any amount of time. On the other hand, in shock experiments the measurements are carried out mostly along the principal Hugoniots which represent the locii of all the points which can be reached by shocking a material from fixed initial conditions[10]. In dynamic shock experiments the time of passage of the shock through the sample is short compared to the disassembly time of the sample. The time available for measurements thus varies from a few microseconds to nano seconds depending upon the method used for generation of shock. The shock compression is not a simple one that occurs in static experiments. The material under shock compression is in fact subjected to shear forces and temperature rise besides rise in pressure. The shock Hugoniot is different from the isotherm passing through the same initial state as shown in Fig. 1. The shock compression imparts higher internal energy to the material compared to the static case which consists of reversible and irreversible internal energy components producing elastic compression and heating of the material, respectively. Thus, as shock compression produces a large thermal component of pressure, the Hugoniot always lies above the isotherm (Fig. 1). The amount of compression produced in a single shock experiment is limited, as at higher shock strengths much of the energy goes into heating rather than to compression. As the Hugoniot traces a different path from an isotherm for the same phase change in a material the transition pressures in the two cases may not match and different phases can be encountered along an isotherm and Hugoniot. Compared to the static situation, shock compression is also accompanied by generation of defects and dislocations. The role played by these defects in shock propagation is not well understood although they are known to act as a nucleation site for the growth of new phase. The time duration of shock experiments is very small compared to the infinite time available in static experiments. The fast rise times and small duration of the shock coupled with the high strain rates that are characteristic of these experiments do not give sufficient time for the growth of a new phase; still, in many cases the polymorphic phase transitions observed to be exhibiting slow kinetics under static loading conditions are found to occur in short times under shock loading and only those phase transitions that have extremely slow kinetics may not get detected during the passage of shock in the material[11,12].

It is thus clear that *in-situ* data on materials under shock conditions is the need of the hour to provide a microscopic understanding of the underlying physical phenomena and to verify the existence of steady state under dynamic situations[13]. The reliability of high-

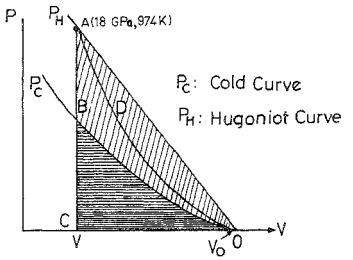

Shock heating; cold compression

FIG. 1. P-V diagram for shock compression of cold material. Vertical lines denote shock heating while the horizontal ones denote cold compression.

Table I
High pressure achieved through various experimental techniques*

Static	*Max. pressure*
Piston-cylinder	50 kbar
Diamond anvil cell (X-ray diffraction)	5 Mbar
Dynamic	
Gas gun	10 Mbar
Lasers	700 Mbar
Underground NE	50,000 Mbar

* see Godwal[16] for details.

pressure data at large compressions is uncertain because the stress state at ultrahigh pressures is not well understood. Shear strength provides a basic description of a material's mechanical behaviour, but very little is known about this quantity at multimegabar pressures[14]. In fact, upon compression, the stress state of all solids is nonhydrostatic when the sample has finite strength. If uncorrected, the presence of shear stresses can lead to systematic errors in physical quantities like bulk modulus and its pressure derivative[15]. Shear strength effects can also introduce errors in measured pressures when secondary calibrants like ruby fluorescence or diffraction standards are used.

Not withstanding these difficulties, by careful experimentation and appropriate modelling, considerable amount of valuable information about behaviour of materials under static and dynamic high-pressure conditions has been obtained. The present article discusses material response under static and dynamic high pressures with interesting results on a variety of new phenomena encountered.

2. Present status of high pressures achieved

In Table I we summarise the present experimental situation for different kinds of experimental systems designed to generate high pressures. It is seen that static high-pressure techniques have reached pressures[16] higher than that at the centre of the Earth (360 GPa) and at the core-mantle boundary (150–200 GPa). Coupling ultrahigh pressures and laser-heating techniques we get close to producing pressure-temperature conditions existing at the centre of the Earth to the core-mantle boundary. Also pressures exceeding 4500 and 1000 GPa existing, respectively, at the centre of the planets Jupiter and Saturn have already been created in the laboratory using giant high-power lasers[17] developed for achieving inertially confined controlled thermonuclear fusion. There have been doubts about the viability of lasers for generation of high-pressure data because of the large error bars associated with determination of pressure from experimentally measured shock velocity. However, recent developments in the area of laser-driven shock waves point to the possibility of obtaining pressure values with accuracies of about 10%[18]. It is also observed from Table I that pressures existing in stars like the white

dwarf can only be produced using nuclear explosions[19] which however require large experimental configurations.

3. Physical phenomena of interest

One of the most important applications of high-pressure research is the study of pressure–volume–temperature relationship of materials, usually known as the equation of state (EOS). In fact, EOS and phase stability are the most fundamental properties obtained from these investigations. Experimental and theoretical investigations of EOS are of immense importance to researchers in both basic and applied sciences. Its utility for meaningful interpretation of physical and chemical phenomena under pressure need not be emphasized. Questions like how the criticality factor for a fissionable mass varies with compression can only be answered with the help of EOS. It provides vital input for hydrodynamic calculations in controlled fission–fusion research, in simulations of reactor accidents and in rock mechanical effects of peaceful nuclear explosions[20–21]. In geophysics it helps to understand the structure of the Earth and in astrophysics to unravel the mysteries of evolution of stellar bodies like white dwarfs, neutron stars and black holes. In the basic sciences it provides the test to the theoretical models of cohesion.

Pressure-induced phase transitions are a very interesting phenomenon and studies of these continue to be one of the most active areas of high-pressure research. With dramatic improvement in the experimental techniques employed in static and dynamic high-pressure research several structural, electronic and insulator-to-metal phase transitions have been observed in various materials[22]. Discovery of crystal-to-amorphous transition in various substances observed under pressure is an interesting example of pressure effect[23]. Another exciting phenomenon observed only under dynamic shock situations is melting and vaporization. It is hoped that it will be possible to reach pressures of 1000 GPa using diamond anvil cell (DAC) in the near future and we expect to observe pressure ionization of inner core electrons in static experiments. So far the combined pressure thermal ionization of core electrons dominated the physical properties along the shock Hugoniots above 1000 GPa.

4. Experimental techniques

The High-Pressure Physics Laboratory at BARC has been engaged in the studies of condensed matter under pressure for about 20 years. Various experimental facilities have been built and used. These include four-probe resistance measurements[24], angle-dispersive X-ray diffraction using WC anvils with Be gaskets[25] and DAC-based full Bragg cone, energy-dispersive X-ray diffraction system (EDXRD) along with a ruby flourescence spectrometer[26] to measure the pressure. Several experimental studies have been carried out on the DAC-based EDXRD system using a white X-ray beam from a rotating anode X-ray generator. The diffracted beam is collected over the full Bragg cone by a conical slit and is energy analysed using a large-area semiconductor (HPGe) detector and indigenous microprocessor-based multichannel analyser. Later, a similar EDXRD system[27] was built and installed at the Institute of Nuclear Physics, Novosibirsk, Russia, at the beam lines of synchrotron radiation source VEPP-3.

A variety of diamond cells have been fabricated at Trombay. The first one to be made was on the design of Syassen and Holzapfel[28]. A DAC, similar to Mao–Bell type, was fabricated for the angle-dispersive diffraction studies using film method[29]. Another DAC which involved a combination of Mao–Bell and Bassett designs[30] was coupled to an indigenous Raman scattering facility[31]. This cell has now been replaced by a Merrill–Bassett[32]-type cell for optical studies. Recently, a Raman setup was built for optical studies at high pressure[33]. This setup has been assembled using a 500-mm single-stage, double-pass scanning monochromator and a super notch filter for 514.4 nm line of Ar ion laser which permits the observation of Raman modes greater than or equal to 100 cm^{-1}. The angle-dispersive X-ray diffraction system incorporating an imaging plate as an area detector has been commissioned[34]. The excellent features of an imaging plate like high sensitivity, dynamic range and linear response makes it most suitable for accurate EOS measurements and for the determination of the structure of high-pressure phases.

In order to study materials under dynamic shock pressures we have set up a compressed gas gun facility at Trombay[35]. In this gun, the projectile, with the impactor mounted on the nose, flies through a barrel to impact the target material to generate a shock wave. The projectile could be accelerated up to 1.2 km/s to generate a peak pressure of about 40 GPa, depending upon the impedance of the impactor and the target.

5. Metallic hydrogen

As hydrogen is the most abundant element in the universe, and is the first entry in the periodic table, its metallization is not only a dramatic illustration of pressure-induced changes in bonding character, but also plays an important role in determining the internal state and evolution of the giant planets. At low pressures, hydrogen crystallizes as an insulating molecular solid and at extreme pressure conditions it forms a dense plasma fluid. Metallic hydrogen is expected to be a high-temperature superconductor[36].

Theoretical studies in the past predicted that under pressure insulating molecular hydrogen will undergo a band overlap transition to a molecular metallic phase before dissociating to form a monoatomic metallic solid. There are wide variations in the predicted pressures for these transitions depending upon the structure, molecular orientation and approximations employed in the theory. Local density approximation (LDA)-based calculations of c-axis-ordered hexagonal closed packed (hcp) phase predict closure of the band gap at 40 GPa[37]. The quasiparticle calculations[38] based on Green's function with screened Coulomb potential (GW) give the value 151 GPa. Lowering the symmetry increases this band gap at 150 GPa[39]. Also, for the monoatomic metallic transition the theoretical predictions range from 250 to 400 GPa[40].

The central problem of hydrogen research at high pressure is the uncertainty of crystal structure. X-ray diffraction on solid hydrogen is the only direct measurement that can give a definite answer on the phase diagram. Hydrogen in the molecular form solidifies at 14 K in the hcp structure at ambient pressure ($V/V_0 = 1$ with V_0 as normal volume).

The past limit of 50 GPa in single-crystal X-ray diffraction[2] studies has been raised to 120 GPa[41]. These measurements demonstrate that hydrogen remains in the hcp structure up to such pressures. The EOS measurements also reveal that the solid hydrogen is enormously compressible[41]. The experiments showed that the crystals became increasingly anisotropic with pressure and that the isotopic shift between hydrogen and deuterium was much smaller than expected.

Dynamic shock experiments have been carried out on fluid hydrogen at Lawrence Livermore National Laboratory by Nellis and coworkers[42]. In these experiments, the EOS and electrical conductivity of fluid hydrogen was measured up to 200 GPa. The measured first shock temperatures up to 20 GPa were in excellent agreement with predictions based on molecular hydrogen. The second shock temperatures up to 90 GPa were lower than predicted for the molecular phase and were due to continuous dissociative phase transition above 20 GPa. The partial dissociation from the molecular to the atomic phase absorbs energy and lowers shock temperatures. In the electrical conductivity measurements high densities and low shock temperatures were obtained using reverberating shock to compress the liquid hydrogen. This avoided dissociation and enabled the measurements of density dependence of band gap closure as the samples were shock-compressed to small temperatures compared to the electronic band gap. In these experiments, the nearly cooled hydrogen provided the semiconducting fluid phase. Shock compression to a high density reduced the band gap while heating the hydrogen sufficiently excited the electronic carriers into the conduction band to produce measurable electrical conductivity. The energy gaps measured were in the density of states of disordered fluid which is claimed to be in the metallic state. These results are important for understanding the physics of metallization of hydrogen and for understanding the isentropes of the interiors of Jupiter and Saturn. The determination of band gap from electrical conductivity measurements of a shocked fluid discussed above is also close to the theoretical and static measurements for the solid phase.

Optical Raman measurements[2,43] show that the hexagonal phase remains stable up to a pressure of 150 GPa ($\rho/\rho_0 = 9$). At this pressure, the measured vibron frequency shows a discontinuity. The nature of this new phase is controversial, although its pressure is in the range of predictions for insulator-to-molecular metal phase transition. Further pressurisation up to 230 GPa indicated that molecular bonds are stable. Above 230 GPa Raman vibron disappeared[44]. The experimental findings further reveal that at around 250 GPa hydrogen begins to absorb visible light consistent with the band gap dielectric model and fits to the index of refraction measurements. However, the ruby R1 peak used for pressure calibration was very weak and difficult to measure.

Disappearance of Raman vibron is consistent with molecular dissociation but not a necessary condition. The dissociation may also be due to pressure-induced absorption of an exciting laser or by fluorescence of a diamond and sample or loss of hydrogen to the anvils. These problems are being investigated by increasing the gasket hole and using a pressure marker in place of ruby. If there is hope for metallization of hydrogen then the pressure has to cross 300 GPa because the refractive index measurements indicate that direct gap closure requires pressure above 300 GPa.

6. Equilibrium shock temperature

When the shock front propagating in a material is assumed to be a sharp discontinuity in stress, then, using the laws of conservation of mass, momentum and energy[10], it can be shown that the undisturbed state is related to the shocked state at the shock front as follows:

$$U_s\rho_0 = \rho_1(U_s - U_p) \tag{1}$$

$$P_1 - P_0 = \rho_0(U_s - U_p) \tag{2}$$

$$E_1 - E_0 = 1/2\ (P_1 + P_0)\ (V_0 - V) \tag{3}$$

where U_s is the shock-front velocity, U_p, the particle velocity in the compressed region, P, E, ρ and $V(= 1/\rho)$ are, respectively, pressure, specific internal energy, density and specific volume, the suffixes 1 and 0 represent quantities in the shocked and the unshocked regions, respectively.

If the equation of state $E = E\ (P, V)$ of the material is also known, we can use (3) to write P as a function of V (P_0 is small and for all practical purposes it is neglected). The locus of all states (P, V) which can be obtained from an initial state (P_0, V_0) is known as the Rankine–Hugoniot (RH) curve (Fig. 1). Measurement of two quantities U_s and U_p determines the shock Hugoniot. It is clear from (3) that the internal energy deposited in the compressed body is the area of the triangle OAC. If the compression is carried out isothermally at zero K to the same final volume V, the material will be at point B. The area of the curved triangle OBC represents the cold elastic energy. The difference between the areas of OAC and OBC represents the heat energy provided by the shock in the compressed sample. The contribution from defects created by the shock, such as vacancies and dislocations, is expected to be small and hence neglected. Measurement of shock temperature is still a burning problem with limited success for a few transparent materials. Information about shock temperatures is obtained from theoretical estimates. Generally, the total internal energy E and pressure P at a given volume are computed as a function of temperature and iterated self-consistently to satisfy eqn (3) to obtain the shock temperature. To illustrate it, a shock pressure of 18 GPa will compress a sample of aluminium from a density of 2.78 to 3.3 g/cm^3 and heat it to 974 K (Fig. 1).

After the shock wave has passed, the material will unload along the curved path ADO. In doing so, it does work on the surroundings, given by the area of the curved triangle ODAC. The difference in the areas OAC and ODAC represents the waste heat deposited on the terminal sample (Fig. 1). If the amount of waste heat exceeds the enthalpy of vaporization (or melting), the terminal sample will be in the vaporized (or molten) state. This interesting phenomenon results from using peaceful nuclear explosion discussed in the following section.

7. Pokhran experiment

India's first peaceful nuclear explosion experiment was carried out on May 18, 1974, in the Rajasthan desert at a place near Pokhran. The aim of the experiment was to study the

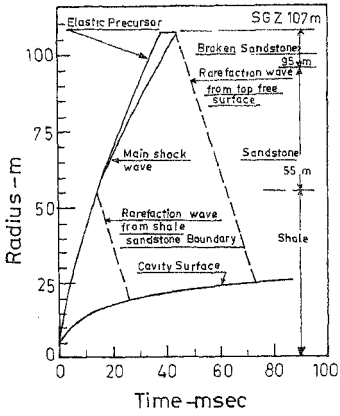

FIG. 2. Computed propagation and cavity growth in vertical direction for the Pokhran experiment.

explosion phenomenology, fracturing effects in rocks, ground motion and containment of radioactivity, etc., in the context of applications of peaceful nuclear explosion. In this experiment, a plutonium device of yield 12 kt equivalent of TNT was emplaced in a shale medium, at a depth of 107 m in a chamber at the end of an L-shaped hole. Upon detonation, the ground surface above the emplacement point rose with a velocity of 25–30 m/s to form a dome 170 m in diameter and 34 m in height. There was no venting of radioactivity in the experiment. The resultant apparent crater, measured with respect to the preshot ground surface, had an average radius of 47 m and a depth of 10 m. This, perhaps, is the only experiment which produced a crater (though shallow), and yet was completely contained from the radioactivity point of view.

Chidambaram and Ramanna[20] have explained the phenomenology of this experiment using computer modelling with an one-dimensional spherical symmetric rock mechanics computer code. The quick release of explosive energy of a nuclear device initiates various physico-mechanical processes in the geological medium, like vaporization, melting, crushing, fracture and motion of the surrounding rock. The reflection of stress waves at the free ground surface imparts additional kinetic energy to the rock medium. Most of the energy of the Pokhran device, as in any other nuclear explosive, was released in less than a microsecond. It has been shown by Chidambaram and coworkers[21] that this resulted in 640 tons of rock, extending up to a radial distance of 6.2 m, which was shock-melted, from the criteria discussed earlier. At the vapour–liquid interface, the pressure is expected to be about 160 GPa. Computed wave propagation and cavity growth are depicted in Fig. 2. The final cavity radius in the horizontal direction is calculated to be about 28–29 m compared to the post-shot measured value of 30 m.

8. Interpretation of shock-wave propagation at atomistic level[45]

In shock-wave experiments usually only two quantities are measured: the shock-wave velocity U_s and the particle velocity U_p due to the passage of the shock wave. Both these quantities are measured with respect to the uncompressed material ahead of the shock front. The interpretation of such data is based on two assumptions. First, the material compressed behind the shock front is assumed to be in thermodynamic equilibrium. This means that stress and energy profiles of the shock wave are steady and enables thermally equilibrated region behind the shock front to propagate with the velocity U_s. Second, the compressed material is assumed to have yielded completely so that the stresses may be assumed to be hydrostatic. An early three-dimensional (3-D) molecular dynamics (MD) calculation carried out by Tsai and Beckett[46] showed nonsteady behaviour and concluded that the RH jump conditions could not be used to analyse data from planar impact experiments. As the equations of motion solved in MD simulations explicitly obey the conservation laws, the test of the validity of RH relations in MD shock simulations is closely connected with the assumption of steady shock wave. In contrast to Tsai and Beckett's[46] findings of nonsteady waves, Paskin and Dienes[47] reported several MD calculations of shock waves in perfect Lennard–Jones crystals at nonzero initial temperature, where only steady waves were observed. A somewhat satisfactory resolution of these discoveries was attempted by Holian and Straub[48]. Their MD calculations of shock waves in perfect three-dimensional solids at nonzero initial temperatures reveal a transition in the nature of the asymptotic shock-wave structure as a function of shock strength. These authors concluded that the key to this transition from nonsteady to steady waves where RH relations are obeyed is the partial relaxation of compressive shear stress behind the shock front which accompanies small but permanent, transverse strains in atomic positions. Pulsed X-ray diffraction experiments in the past on LiF crystals with tens of nanosecond time resolution and shocked using explosive or gas gun drivers established that the compression of single crystals by shock waves is hydrostatic and therefore plastic on those time scales, but in a manner which somehow preserves single-crystal orientation[4]. However, later experimental measurements up to a few tens of kilobar support the view that the immediate response should be elastic and uniaxial[49–50]. In these studies it was not possible to determine a transverse component of strain (although it was found in polycrystalline samples of aluminium[51]) but the recent measurements of Whitlock and Wark[5] reveal that definite compression was recorded in the inertially confined transverse direction indicating the onset of plastic lattice response. It thus appears that steady shock conditions are attained for strong shocks or for weaker shocks at nonzero temperatures. Fritz[52] using a relaxation time of about ps and a shock velocity of 7–10 km/s found that a typical sample thickness of 1 mm corresponds to 10 relaxation lengths. The MD calculations show that thermal equilibrium is established within a few tens of lattice parameters behind the shock front[53]. It is thus emphasized that at low pressures the time-dependent response of shock in condensed matter should be considered.

It is expected that there will be a large concentration of defects, like vacancies, dislocations, etc., in the shock-compressed material[54]. In the description of propagation of

shock in Meyers' model[55]—a modification of an earlier model by Smith[56]—and Mogilevsky[57], dislocations are homogeneously nucleated at or close to the shock front by the deviatoric stresses in the material which in turn are relaxed by the generation of these dislocations. There is controversy regarding the speeds with which the dislocations move but the heating by them seems to be an important energy-dissipative mechanism[58]. The dislocation density in recovered samples is typically 10^{10}–10^{11} cm^{-2} at pressures up to about 10–20 GPa but seems to decrease in shock-loaded copper at still higher pressures due to increased residual temperature leading to annealing effects. The combination of residual and active measurements also seems to provide evidence for typical vacancy concentrations from 10^{-5} to 10^{-2} in a pressure range up to few tens of GPa. The pressure correction needed for EOS data due to defects volumes is not well understood.

In the range of pressures from a few hundred kilobars to multi megabars the material behaviour is well understood using first-principles theories. In fact, incorporating their predictions for total energy and pressure in RH relations has led to the determination of shock P–V curves in various materials in excellent agreement with experimental Hugoniots measurements. The various predictions made by these theories are still being verified by current state-of-the-art experiments[59] and we suggest the reviews by Godwal *et al.*[60] and Ross[61] for details.

In the lower pressure region (hundred kilobars or so) the use of RH equations is best at suspect because of nonsteady shock. The use of perfect crystalline solids is far from reality as it is impossible to eliminate defect generation as the shock propagates. Although nonsteady shock behaviour is observed in MD simulations the incorporation of defects in such attempts seems to be extremely difficult to know the changes brought about. Also the first-principles simulation based on coupled density MD approach lacks the required accuracy due to limitations on the number of atoms which can be simulated. Conditioned by these constraints we have thought of a model for shock propagation in solids in the regime of nonsteady waves[45]. We assume that an instantaneous response of materials to impact is uniaxial from its initial undisturbed state. We feel that relaxation mechanisms like phonon-mediated ones as noticed in MD simulations will drive the system to an equilibrium state which could be a nearly hydrostatically compressed state. The model is schematically depicted in Fig. 3. We assume that the difference in free energy between uniaxially compressed state and hydrostatic state appears as irreversible heat and causes excitations of ionic and electronic degress of freedom and gives rise to shock temperature. In fact, we have carried out first-principles total energy calculations for Al using the energy band structure method. The computations were carried out in body-centered tetragonal (bct) phase to allow for uniaxial and hydrostatic states B and C as shown in Fig. 3. The details of such studies will be published elsewhere[45]. Nevertheless in Table II we compare the calculated temperatures with those obtained from the use of first-principles prescriptions for total internal energy and pressure in RH relations. The values seem to differ more for higher pressures. This is due to the fact that isotropic behaviour prevails at high shock strengths. Also our assumption of hydrostatic strain can be objectionable.

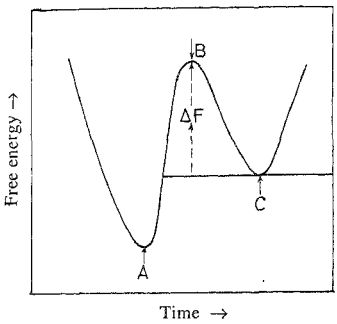

FIG. 3. Schematic of shock compression model. Points A, B and C in free energy *vs* time graph represent uncompressed, uniaxially compressed and hydrostatically compressed states

Table II
Predictions of shock model for Al
(Time of relaxation : pico second)

Pressure (GPa)	Shock temperature (Degree K)	
	Nonequilibrium model	Equilibrium model
9.4	490	450
18	974	915
37 6	1044	980

9. Examples of phase transition

In the area of phase transitions a large number of studies have been made on different substances using various experimental tools mentioned above[62]. The details of such studies have been discussed in various articles[22,62]. In the present article we will discuss a few examples for which the theory has provided the basic underlying mechanism and which otherwise is not available from the experiments.

Thorium crystallizes in the face-centered cubic (fcc) structure at ambient conditions. Vohra and Akella[63] using energy-dispersive X-ray diffraction with DAC found that it undergoes an fcc-to-bct structural phase transition at 80 GPa (Fig. 4(a)). With the help of energy band structure calculations, Rao *et al.*[64] studied the 5-f band characteristic through the fcc-to-bct transition and analysed the angular momentum decomposition of occupied electron states, and the position of the 5-f band with respect to the Fermi level E_F. We found that the 5-f band population increases with pressure, with the band containing more than one electron per atom at the volume fraction of 0.6. We also found from details of the energy band structure[64] that this transition occurs when the bottom of the 5-f band falls below the Fermi level as shown in Fig. 4(b). Due to the proximity of this crossing to the fcc–bct transition, it is reasonable to conclude that the f-band occupation is central to this structural transition.

Several substances have been found experimentally to show crystal-to-amorphous phase transition under pressure. One such example[23,65] which initiated several studies on amorphization at Trombay is $LiKSO_4$. The EDXRD patterns of this compound under increasing pressure are shown in Fig. 5(a–c). As the pressure is increased, a broad glass-like background increases with a simultaneous decrease in the intensity of Bragg lines.

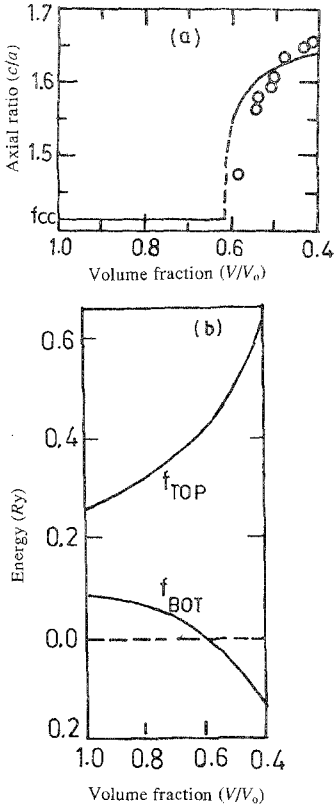

FIG. 4.(a) Axial ratio c/a vs V/V_0 for thorium. The c/a values correspond to the minimum of the total energy curves at various volume fractions. Circles represent experimental data from Vohra and Akella[63], (b) Position of the 5-f band relative to Fermi energy E_f in thorium at various compressions.

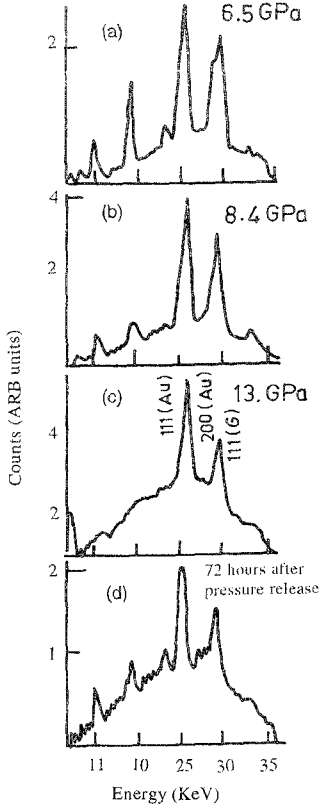

FIG. 5(a–c). Diffraction patterns of $LiKSO_4$ recorded at different pressures. 5(d) is recorded after the release of pressure[23].

The diffraction pattern completely disappeared at about 13 GPa. The peaks which are still seen are due to Au pressure marker and gasket. It is seen from Fig. 5(d) that the crystalline form re-emerges on release of pressure after about 72 hours.

The cause of this transition is due to the fact that $LiKSO_4$ has a stuffed tridymite structure with three-dimensional networks built of six-membered rings of vertex-linked LiO_4 and SO_4 tetrahedra with K in large open interstices. It is well known that coordination polyhedra, joined at vertices, have several configurations, with different relative orientations of polyhedra but with roughly the same energy. Also the possibility of different polyhedra having different compressibilities explains the abundance of phase transition caused by polyhedra tilting. This coupled with the fact that under pressure the tendency to have increased coordination, and kinetic constraints drive the system towards a kind of frustration resulting in amorphization. We refer to a recent reveiw article by Sharma and Sikka[65] for an up-to-date account of the developments on amorphization.

Zn is unique among hcp metals, having unusually large c/a axial ratio at ambient condition ($c/a = 1.856$). The anomaly in the variation of the axial ratio with pressure was first reported by Lynch and Drickamer[66] around 7 GPa. They also reported an anomaly in electrical resistance in the same pressure range. Schulte *et al.*[67], on the other hand, have found no anomaly in the axial ratio when studied using energy-dispersive X-ray diffraction up to a pressure of 32 GPa. The existence of anomaly in the axial ratio of Zn is thus controversial.

Meenakshi *et al.*[68] calculated the change in the axial ratio of Zn under pressure from first-principles total energy calculations. The axial ratio at various compressions is obtained from minimization of total energy. It was noticed that volume dependence of the axial ratio changes slope around the relative volume of 0.92 (Fig. 6(a)). By careful analysis of the computed density of states as a function of compression, they came to the conclusion that the anomaly is related to the appearance of maximum in the density of states at the Fermi level.

Takemura[69] has recently carried out angle-dispersive X-ray diffraction measurements on Zn for its axial ratio (c/a) variation with pressure using a DAC, synchrotron radia-

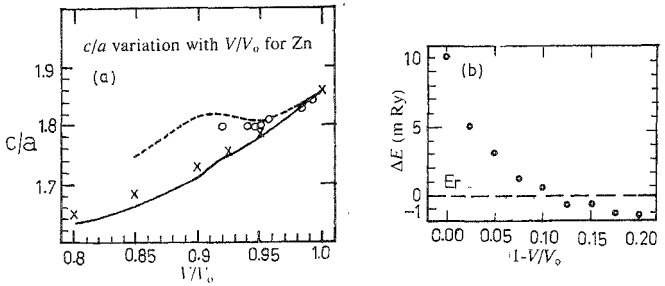

FIG. 6.(a) The c/a variation with V/V_0 for Zinc The solid line is calculated from total energy calculations and is compared with experimental data sets[67]. (b) The falling of energy level of L point in BZ below the Fermi level around $V/V_0 = 0.9$[70].

tion, and an imaging plate. It was revealed that the volume dependence of the c/a ratio changes the slope at $V/V_0 = 0.893$. Also, in the recent past, Potzel *et al.*[70] detected an anomaly in the Mossbauer spectrum of Zn at 6.6 GPa and 4.2 K. The anomaly is accompanied by a drastic change of the lattice dynamics. The scalar-relativistic linear-augmented plane wave calculation verified that the anomaly is related to the topological change of the Fermi surface around the L-symmetry point of the Brillouin zone. Thus the cause of the anomaly in the volume dependence of axial ratio is the electronic topological transition (ETT) as revealed in Fig. 6(b).

10. Symmetry systematics of pressure-induced phase transitions

The pressure increases the repulsive forces between neighbouring atoms and leads to an increase in the potential barrier. As the atoms have to overcome this barrier in order to diffuse it is thought that most pressure-induced phase transitions are diffusionless[71]. Because of this, there exists a one-to-one correspondence between the positions of atoms in the parent and the product phases and is displayed in the interesting symmetry relationship. Based on this relationship, Gupta and Chidambaram[72] have classified pressure-induced phase transitions into four categories: (i) iso-symmetric transition, an example of which is alpha-to-beta phase change in molecular substance resorcinol at a pressure of 0.5 GPa[73-74], (ii) intersection group transition (for

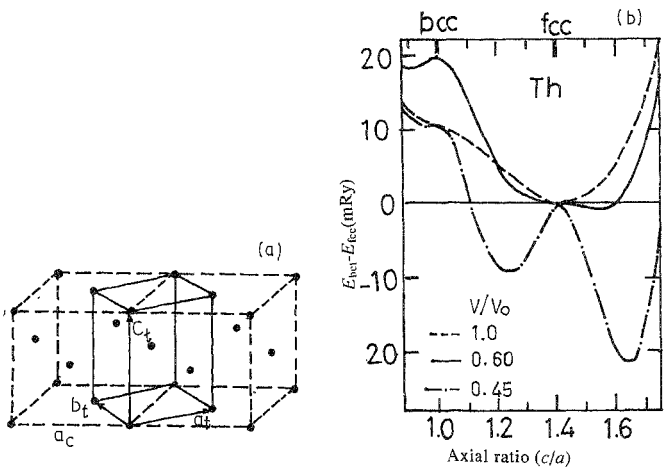

FIG. 7.(a) The fcc structure represented as a bct cell. (b) Total energy E_{bct} of thorium in the bct structure (relative to that in the fcc phase), calculated as a function of axial ratio c/a. The curves of various compressions are as indicated in the legend.

example, omega-to-beta transition[75] in Zr at 32 GPa), (iii) order–disorder transition[76] and crystalline-to-amorphous phase changes[65] fall in this class, and (iv) group–subgroup transition; for example, Th which undergoes fcc–bct structural phase change[63,64].

Thorium has a space group Fm3m, at ambient conditions. As discussed earlier, the high-pressure phase transition occurs to bct phase with space group I4/mmm. There is no volume change in this transformation. As seen in Fig. 7(a) the ambient fcc structure of Th can be represented in a bct unit cell with $a_t = a_c/\sqrt{2}$, $c_t = a_c$ and $c_t/a_t = 1.414$, where a_t and c_t are the lattice parameters for the bct phase. Figure 7(b) shows the behaviour of total energy as a function of axial ratio obtained by Rao *et al.*[64] using the energy band method. The single minimum observed at normal volume shifts to a higher c/a ratio at high compressions. Symmetry systematics of various pressure-induced transitions observed by us under pressure are discussed by Gupta and Chidambaram[72].

11. Predictions of phase transitions

The development of *ab-initio* total energy calculations and first-principles molecular dynamics simulations have been going through rapid expansions during the last decade, with the development of many diverse techniques to reduce the computational times[77–80]. The aim of these calculations has been to predict accurately structures and related ground state properties of solids without using any information from the experiment. These include calculations of lattice constants of crystals; elastic, dielectric, and piezoelectric constants; phonon frequencies; pressures for transitions between different phases; and structures of complex crystals[81–83]. The other quantities not known experimentally have also been predicted, such as energies of nonequilibrium phases, the energy of solid along a continuous path connecting stable phases; eigenvectors of phonons; nonlinear elastic properties and structures of surfaces and interfaces[84,85]. There are three main developments which have led to the growth of first-principles calculations. The first is the enormous increase in computational power which has made possible computations on real materials. The high accuracy achieved has enabled their detailed meaningful comparison with experimental measurements. Also, it has provided new tools for attacking the fundamental many-body quantum-mechanical problem. The second important development is the density-functional method for electron exchange and correlation. This method has made it feasible to calculate the above-mentioned ground state quantities with remarkably accurate results for real solids. In fact, it has become the starting point for almost all current first-principles calculations of total energies of solids. Many formalisms like *ab-initio* pseudopotential method (AP)[86], generalized pseudopotential theory (GPT)[87], linear augmented plane wave (LAPW)[88] and linear muffin-tin orbital (LMTO)[89] method are used for the calculation of total energies of solid as a function of pressure from details of band structure calculations. The recent development of techniques for direct minimization of total energy using density-functional method[90] further enhanced the speed of computation. Finally, there are significant new developments in experimental techniques and material preparation in ways never before realized. The most important advance is the ability to create multimegabar pressures and explore the

properties of matter over a wide range of densities[91–95]. In static high-pressure studies, the use of novel DAC incorporating excellent features of imaging plate two-dimensional area detector with rotating anode X-ray generator and at synchrotron facilities has enabled the detection of new phase transformations in solids at ultrahigh pressures[96,97]. In the area of dynamic shock waves a new technique[98] is used in which the phase transformation is inferred from the observation of a discontinuity in the measured sound velocity as a function of peak pressure in the shocked state. The detection is macroscopic in nature and the microscopic details of the transition are obtained either by comparison with the static measurements or from theoretical calculations[99–101]. The high-pressure data obtained thus provides a testing ground for the theory. In addition, there are new fields of research in which the electronic structures play a dominant role, yet are largely unknown experimentally. For example, semiconductor surfaces, where theoretical predictions have stimulated experiments and led to significant changes in understanding the nature of the surfaces[85]. *Ab-initio* total energy calculations have been very successful in predicting phase transitions under pressure prior to their confirmation by experiments. Silicon at ambient conditions is a tetrahedrally coordinated semiconductor with a diamond structure. In 1980, Yin and Cohen[102], using AP, showed that, starting with the atomic number of silicon, a precise estimate of the total energy of solid can be generated composed of specific arrangements of silicon cores of charge 4 embedded in a sea of itinerant valence electrons. The list of candidate structures used for various core arrangements consists of diamond, hexagonal diamond, white tin, simple cubic, bcc, hcp and fcc. Several other structures were also tried; however, the diamond structure was found to have the lowest energy. The calculated lattice parameter and bulk modulus (its pressure derivative) agreed with experiment to within 0.4 and 1%, respectively. Yin and Cohen[102] further showed that at reduced volumes (pressure 10 GPa) silicon should be metallic and stable in white tin form and in hexagonal close-packed structure at 40 GPa. Although the white tin transition was known, the stability of hexagonal close-packed structure was a prediction. Experiments were then carried out and the predicted structure was found at estimated pressure. When the calculations were extended to compute the lattice vibrational properties and the interactions of the valence electrons with the vibrating core, it was found that simple hexagonal silicon should be superconducting at temperatures in the 5–10 Kelvin range and that hcp silicon would be superconducting around 4–5 Kelvin. This provided a successful prediction of the existence of high-pressure phases, their lattice constants, electronic and lattice properties, and superconductivity. This was remarkable in view of the fact that the calculations required only atomic number, atomic mass and candidate structures as input. Many systems have been studied with similar success. For example, the simple hexagonal structure of germanium was successfully predicted to be stable around 84 GPa and the hcp structure around 105 GPa using total energy pseudopotential calculations[103,104] and was experimentally verified[105]. McMahan and Moriarty[106] predicted hcp-to-bcc phase transition in Mg at 50–57 GPa which was observed in DAC experiments at 50 GPa[107]. The phenomenon of theoretical predictions and their subsequent verification by experiments was repeated in Zr[75] and Pb[108]. The theory has also played an important role in removing the controversies existing in various experiments. The interesting example is found in Mo where the

controversy arising between static and dynamic high-pressure experiments is resolved from theory[101]

As part of our program to investigate materials for their phase stability at high pressures, various studies have been made and reported using energy band methods in the past[22,109]. In the present article, we discuss a few recent examples which still continue to attract researchers.

Current first-principles calculations using ASA–LMTO[64] and full-potential LMTO[109] calculations show that Th is not an spd metal as believed earlier but it has contribution to its bonding from 5-f band. This was verified by Rao *et al.*[110] by carrying out total energy calculations with 5-f electrons not contributing to metallic bonding by restricting the muffin-tin-orbital expansion of the electron wave function up to angular momentum $l = 2$. This leads to the stabilization of the bcc phase at ambient conditions and continues to remain stable through the volume fraction of $V/V_0 = 0.4$. Hence, Rao *et al.*[110] were the first to show that the itinerant 5-f electrons were essential to stabilize the fcc structure. These findings have been confirmed by Johansson and coworkers using full-potential LMTO calculations[109]. The computed isotherm with and without inclusion of 5-f electrons is compared in Fig. 8 with the experimental data of Vohra and Akella[63]. It can thus be concluded that it is wrong to consider thorium as a traditional tetravalent *d* transition metal belonging to the same group of elements as Ti, Zr and Hf. The observed fcc structure and the EOS is consistent with the view that Th should be considered as an spdf metal belonging to heavier actinide metal group (Pa–Pu).

The phase diagram of Ti, Zr and Hf has been of considerable interest in the recent past, both experimentally and theoretically. McQueen *et al.*[111] in shock experiments noticed discontinuities in their shock velocity *vs* particle velocity plots at 17, 26, 40 GPa, respectively. Many speculations have been made to explain these discontinuities. McQueen *et al.*[111] assumed that these were due to an alpha (hcp) to beta (bcc) transition, based on the observation of beta phase in shock-recovered samples of Ti. Kutsar and

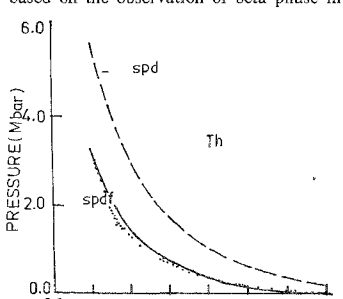

FIG. 8. OK isotherm of thorium compared to experimental data. The curve marked spd is for the case when f electron contribution is suppressed in the calculation.

German[112] associated these with the alpha-omega (omega, a three-atom simple hexagonal structure) as the omega phase was found by them in shock-recovered samples of Ti and Zr. Carter[113], on the other hand, thought that these could be due to some electronic transition.

These controversies motivated Gupta *et al.*[114] to carry out electronic structure calculations on these materials using ASA–LMTO method. For example, in Zr they correctly found the alpha structure as the most stable one at normal volume which continued to remain so till 5 GPa pressure where it transforms to an omega structure as compared to the experimental transition pressure of 2–6 GPa. Also, a new omega-to-beta structural transition at higher pressure (Fig. 9) was predicted. This was subsequently observed in static experiments at 30 GPa. Thus the cause of the shock discontinuity in Zr has been attributed to this transition.

Alpha-quartz form of SiO_2 exists at room temperature and up to pressures less than 7 GPa. With increase of pressure, it persists as a metastable structure, undergoes a transition to another metastable structure before making transition to an amorphous phase around 20 GPa (see Sharma and Sikka[65] for more details). The shock experiments show a break in the Hugoniot around 15–20 GPa and the recovered samples contain amorphous material. In shock waves there has been a controversy regarding the nature of the transition. In fact, it has been interpreted as alpha-quartz-Stishovite phase change.

In the recent past, first-principles electronic band structure calculations[115] and molecular dynamic simulations[116] based on force fields derived from quantum mechanical studies have been made to understand the various aspects of this crystal to amorphous transition like change of bonding, coordination and driving mechanism, etc. Chelikowsky *et al.*[115] and Di Pomponio and Continenza[116] reproduced well the variations of V/V_0, Si–O–Si and O–Si–O angles as well as interpolyhedral O—O distance in alpha quartz as a function of pressure, respectively, using self-consistent pseudopotential method and LAPW technique. In fact, the interpolyhedral O—O distance has the shortest value of 2.7 Å at 15 GPa in silicates. This is considered as the cause of the instability of the alpha-quartz structure because the compression beyond will be very expensive in energy. The calculated pressure *vs* V/V_0 curve by Somayazulu *et al.*[117] using molecular dynamic simulations is compared with experimental data in Fig. 10. It is seen that the agreement with the data in the crystalline phase is excellent. At higher pressures, the EOS of the simulated amorphous phase is close to that of the shocked alpha-quartz. It is also revealed from Fig. 10 that the unloading path is much steeper which is similar to the observations of release wave measurements in the shock experiments on X-cut quartz.

The above examples show that theories play a powerful role in the predictions and interpretations of high-pressure phenomena. The introduction of linear band structure methods like LMTO and LAPW techniques for total energy calculations have enhanced their computational efficiencies by at least one order of magnitude. However, even when such methods are used, the calculations become extremely time consuming when the Hamiltonian matrix size increases beyond 300 by 300 (especially, when the periodic unit cell in the solid contains many atoms). Nevertheless, with the availability of supercom-

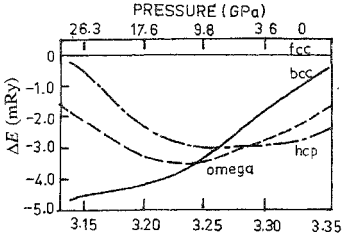

FIG. 9. Calculated structural energy differences for Zr[114].

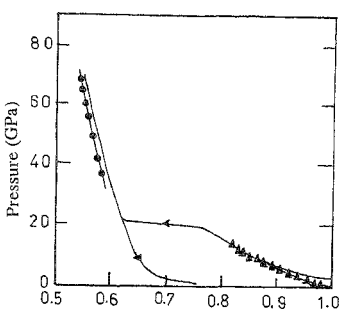

FIG. 10. Pressure–volume relation for quartz SiO_2 is shown with expenmental data[117].

puters and parallel-processing machines as an alternative, it is possible to carry out state-of-the-art electronic structure calculations for novel materials. In fact, we used the recently developed parallel-processing system at BARC referred to as BPPS[118] to perform electronic structure calculations on ©-$Mg_{32}Zn_{48}$ where © denotes the central site of packing unit, with Zn, Mg, Al and vacancy at ©. We employed the parallelized LMTO program[119] and the calculations in the bcc structure are related to 1/1 crystal approximant to the Al–Zn–Mg quasicrystal. Based on total energy calculations[120] it was found that packing units with Al or Zn at the centers are more stable than those with empty centers, supporting the positron annihilation findings of Chidambaram and coworkers[121].

The density functional-based first-principles total energy calculations can determine the most stable structure from the chosen candidate structures, but might fail to locate the structure that has the lowest free energy. This problem has so far been attempted by intelligent search. However, using the density functional molecular dynamics[90] approach it is possible to discover the equilibrium structure. Moreover, the Kohn–Sham equations-based electronic structure calculations can be applied mainly to pure crystals with ASA–LMTO and full-potential LMTO to be employed, respectively, for closed packed and less closed packed systems.

It is desired to have the first-principles electronic studies for complex materials in order to understand various physical phenomena. These include dynamics of materials, structure of solid surfaces and grain boundaries, structure of clusters, and defects and impurities in solids. In many of these complex tasks, the empirical potentials may not be reliable, or are difficult to construct. In the first-principles attempts to study some of these properties, for example, by employing supercells, the methods based on eigenvalue evaluation of the Hamiltonian matrix severely limits the system size. The number of ba-

sis states required would increase linearly with the number of atoms, and the computational demands would increase at least as a cube of the total number of basis states. Hence, the first-principles molecular dynamic calculations would be impossible for more than ten atoms. The main drawback, inherent in the diagonalization and related schemes of finding matrix eigenvalues, is that one has to carry out the calculations for unoccupied electron states also, though not used anywhere in the self-consistent process. This may reduce the efficiency of computation by an order of magnitude. Alternatively, the direct minimization of total energy keeps track of occupied electron orbitals only. The basic idea is to consider the total energy as a function of all the wavefunction coefficients of occupied electron states, and ionic positions. Starting with any arbitrary set of trial electron orbitals, one can iteratively upgrade them to get the minimum of total energy. In principle, any minimization scheme can be employed, and the set of one-electron orbitals corresponding to the minimum total energy represent the Kohn–Sham orbitals. In order to study the dynamics of ions, their positions can be included as additional variables, and the structural relaxation can be treated as a global minimization problem, for example, by simulated annealing technique[122]. Car and Parrinello[90] treated the many-body quantum mechanical problem on the same footing by using coefficients of electron wave functions and ionic positions as though they formed a dynamical system and the corresponding phase space is explored by molecular dynamics simulations.

We have implemented the coupled density functional molecular dynamics scheme for simulations by the Car–Parrinello (C–P) method on BPPS[123,124]. The program employs the easy space evaluation of various quantities in the calculations of total energy and force which leads to frequent transformations between reciprocal and direct spaces. Hence, the direct and inverse fast Fourier transforms (FFTs) are called often in each MD time step. Therefore, we parallelized the FFT routines and the results of a test simulation for Sn dimer were compared with Convex-220 machine to check the reproducibility on BPPS. By employing assembler-coded FFTs on BPPS with 8 nodes a speed up of 4 is achieved[124]. The inclusion of soft potentials, commonly known as Vanderbilts potentials[125], in C–P method and the use of separate heat bath for electrons have increased its applicability to complex solids and metallic systems[126–127].

First-principles simulations involving variable cells are currently being carried out to compute thermodynamic properties and phase stability of materials[127,128]. Attempts to locate the solid–liquid–solid boundary have been made for computing the change in physical properties of materials upon melting.

We have applied the C–P method to study the molten phase of sulphur and currently the first-principles simulations are being carried out to investigate the structure of its amorphous phase under pressure as there is controversy about its structure[129].

12. Conclusions

The extensive high-pressure data obtained using static and dynamic methods along with the development of theoretical means has contributed significantly to the understanding

of condensed matter physics. The need to have a proper agreement between theory and experiment has led to the incorporation of gradient correction[130], self-interaction terms and nonlocal effects[131] in LDA. In fact, the generalized gradient correction of the exchange and correlation energy has been shown to correct qualitative errors of LDA in describing a high-pressure phase transition of SiO_2 in excellent agreement with experiments[132]. From the conclusions of recent reviews[133-134] on this subject it is now well accepted that the first-principles total energy calculations have proved to be a powerful means of providing valuable information on material behaviour under static and dynamic pressures. In fact, a long-standing goal of condensed matter physics, namely, prediction of phase transformations of real materials from first-principles microscopic quantum mechanical theory has been achieved. The theory has also been very successful in resolving controversies in different experimental data and on several occasions it has helped in reinterpretation of experiments. Some efforts have been made to generate the parameters of the empirical potentials by first-principles electronic structure calculations for the ionic configurations appropriate to MD simulations. The deviations of trajectories obtained by MD and first-principles simulations for small sample size, for example, by C–P scheme, will indicate changes in the bonding characteristics and help to improve the empirical potentials during the course of large-scale MD simulations. This is essential when making and breaking of bonds is involved or when core ionization occurs at ultrahigh pressures.

The precise DAC experiments are eagerly awaited in the pressure range of 300 GPa to confirm the metallization of hydrogen. The optical and X-ray diffraction measurements with pico second time resolution shall provide an insight into the atomic-molecular processes governing the shocked state and because of the fast temporal nature of shock-wave loading, time-resolved measurements shall permit real-time examination of structural and chemical changes due to well-defined large compressions. The interpretation of such experiments by theory shall provide an insight into the microscopic mechanisms accompanying shock propagation in condensed matter. It appears that the goal of shock wave research to measure precisely the shock temperatures shall be fulfilled by finding proper sample/window interface specially for opaque substances and with use of pico-second time-resolved optical spectroscopy[135]. With the availability of static pressures higher than those at the centre of our planet, it is hoped that materials of geophysical interest, coupled with laser heating and synchrotron radiation, will be an active area of high-pressure research in the near future and will provide direct comparison between static and dynamic high-pressure data.

In short, research on substances at high pressures has developed into an interdisciplinary area with important implications for basic and applied sciences.

Acknowledgement

I am deeply grateful to Dr B. K. Godwal for numerous discussions on the contents of this article and for help in its preparation. I am also thankful to Dr S. K. Sikka and other members of the High Pressure Group; in particular, Drs S. C. Gupta and S. M. Sharma for helpful discussions.

References

1. JAYARAMAN, A. — *Rev Mod Phys*, 1983, **55**, 65.
2. MAO, H. K. AND HEMLEY, R. — *Rev Mod Phys*, 1994, **66**, 671.
3. DUVALL, G. E. AND GRAHAM, G. A. — *Rev. Mod. Phys.*, 1977, **49**, 523.
4. JOHONSON, Q. AND MITCHELL, A. — *Phys. Rev Lett.*, 1972, **29**, 1369.
5. WHITLOCK, R R. AND WARK, J. S. — *Phys. Rev. B*, 1995, **52**, 8.
6. BOTELER, J. M. AND GUPTA, Y. M. — *Phys. Rev. Lett.*, 1993, **71**, 3497.
7. WARK, J. S., WHITLOCK, R. R., HAUER, A , SWAIN, J. E. AND SOLONEOL, P. J. — *Phys Rev. B*, 1987, **35**, 9391.
8. YOO, C. S., AKELLA, J. AND MORIARTY, J A. — *Phys Rev. B.*, 1993, **48**, 15529.
9. GODWAL, B. K., MEADE, C., JEANLOZ, R., GARCIA, A., LIU, A Y. AND COHEN, M. L. — *Science*, 1990, **248**, 463.
10. ZEL'DOWICH, YA. B. AND RAIZER, YU. P. — *Physics of shock waves and high temperature hydrodynamic phenomena*, Vols 1 and 2, 1967, Academic Press.
11. JEANLOZ, R. — *J Geophys. Res.*, 1987, **92**, 10352.
12. SIKKA, S. K. — *Bull Mater. Sci.*, 1992, **15**, 35.
13. HOLIAN, B. L. AND STRAUB, G. K. — *Phys. Rev. Lett.*, 1979, **43**, 1598.
14. DUFFY, T. S., HEMLEY, R. J. AND MAO, H. K. — *Phys. Rev. Lett.*, 1995, **74**, 1371.
15 JEANLOZ, R., GODWAL, B. K. AND MEADE, C. — *Nature*, 1991, **349**, 687.
16. GODWAL, B. K. — *Curr. Sci.*, 1995, **68**, 1087.
17. CAUBLE, R *et al.* — *Phys Rev. Lett.*, 1993, **70**, 2102.
18. KOENIG, M *et al.* — *Phys. Rev. Lett.*, 1995, **74**, 2260.
19. VLADIMIROV, A. S. *et al.* — *JETP Lett.*, 1984, **39**, 82.
20. CHIDAMBARAM, R. AND RAMANNA, R. — *Proc, Tech. Commun. PNE IV*, Vienna, International Atomic Energy Agency, 1975, p. 421.
21. CHIDAMBARAM, R., SIKKA, S. K. AND GUPTA, S. C. — *Pramana*, 1985, **24**, 245.
22. CHIDAMBARAM, R. AND SHARMA, S. M. — *Curr. Sci.*, 1991, **60**, 397.
23. SANKARAN, H., SIKKA, S. K., SHARMA, S. M. AND CHIDAMBARAM, R. — *Phys. Rev. B*, 1988, **38**, 170.
24. VIJAYAKUMAR, V., GODWAL, B. K., SIKKA, S. K. AND CHIDAMBARAM, R. — *J Phys. F Met. Phys.*, 1984, **14**, L65.
25. VOHRA, Y. K., VIJAYAKUMAR, V., GODWAL, B. K., SIKKA, S. K. AND CHIDAMBARAM, R. — *Rev. Sci. Instrum.*, 1984, **55**, 1593.
26. SIKKA, S. K., *et al.* — *Indian J Pure Appl Phys.*, 1989, **27**, 472.
27. SIKKA, S. K., MOMIN, S. N., VIJAYAKUMAR, V., TALACHKO, B. P. AND CHIDAMBARAM, R. — *Solid St Phys C*, 1993, **35**, 86.

28. HUBER, G., SYASSEN, K. AND HOLZAPFEL, W. B. — *Phys. Rev*, 1977, **15**, 5123.

29. GODWAL, B. K., JAYARAMAN, A., MEENAKSHI, S., RAO, R. S., SIKKA, S. K. AND VIJAYAKUMAR, V. — *Solid St Phys C*, 1994, **37**, 423.

30. VIJAYAKUMAR, V., MEENAKSHI, S., GODWAL, B. K., SIKKA, S. K. AND CHIDAMBARAM, R. — Recent trends in high pressure research, *Proc. XIII AIRAPT Int Conf. on High Pressure Science and Technology*, (A. K. Singh, ed.), Oxford and IBH, New Delhi, 1992, p. 331.

31. ROY, A. P. AND BANSAL, M. L. — *Indian J Pure Appl. Phys.*, 1988, **26**, 218.

32. MEENAKSHI, S., GODWAL, B. K. AND SIKKA, S. K. — The ruby response of an indigenously developed Merrill-Bassett type cell has been studied up to the pressure of over 10 GPa. The cell is being used for optical studies (unpublished).

33. CHITRA, V., MOMIN, S. N., KULSHRESHTHA, S. K. AND SHARMA, S. M. — *Solid St. Phys C*, 1995, **38**, 359.

34. MEENAKSHI, S., GODWAL, B. K., VIJAYAKUMAR, V., RAO, R. S., JAYARAMAN, A. AND SIKKA, S. K. — *Solid St Phys C*, 1995, **38**, 367.

35. GUPTA, S. C. *et al.* — *Shock compression in condensed matter*–1991 (S. C. Schmidt, K. D. Dick, J. W. Fowles and D. G. Tasker, eds), p. 834, 1992, Elsevier.

36. WIGNER, E. AND HUTINGTON, H. B. — *J. Chem. Phys*, 1935, 3, 764

37. BARBEE, T. W., GARCIA, A., COHEN, M. L. AND MARTINS, J. L. — *Phys. Rev. Lett.*, 1989, **62**, 1150.

38. CHACHAM, H. AND LOUIE, S. G. — *Phys Rev. Lett.*, 1991, **66**, 64.

39. KAXIRAS, E., BROUGHTON, J. AND HEMLEY, R. J. — *Phys. Rev Lett.*, 1991, **67**, 1138.

40. NAGARA, H. AND NAKAMURA, T. — *Phys. Rev. Lett.*, 1992, **68**, 2468.

41. LOUBEYRE, P. *et al.* — In *Proc. 1995 AIRAPT Conf. on High Pressure Science and Technology*, Warsaw, Poland (to be published).

42. NELLIS, W. J., HOLMES, N. C., ROSS, M. AND WEIR, S. T. — In *Proc.* 1995 *AIRAPT Conf. on High Pressure Science and Technology*, Warsaw, Poland (to be published).

43. SILVERA, I. — In *Proc.* 1995 *AIRAPT Conf. on High Pressure Science and Technology*, Warsaw, Poland (to be published).

44. MAO, H. K. AND HEMLEY, R. J. — *Science*, 1989, **244**, 1462.

45. GODWAL, B. K. AND CHIDAMBARAM, R. — Atomistic model for shock propagation in condensed matter, to be published, 1996.

46. TSAI, D. H. AND BECKETT, C. W. — *J Geophys. Res.*, 1966, **71**, 2601.

47. PASKIN, A. AND DIENES, G. J. — *J Appl. Phys.*, 1972, **43**, 1605.

48. HOLIAN, B. L. AND STRAUB, G. K. — *Phys. Rev B*, 1978, **18**, 1593.

49. TUNISON, K. S. AND GUPTA, Y. M. — *Appl. Phys. Lett.*, 1986, **48**, 1351.

50. VORTHMAN, J. E. AND DUVALL, G. E. — *J. Appl Phys.*, 1982, **53**, 3607.

51. AL'TSHULER, L. V. AND EGAROV, L. A. — *JETP*, 1981, **54**, 359.

52. FRITZ, J. N. — *High pressure science and technology*, Vol. 1 (B. Vodar and Ph. Marteau, eds), p. 263, 1980, Pergamon Press.

53. TSAI, D. H. AND MACDONALD, R. A. — *High Temp. High Pressures*, 1976, **8**, 403.

54 CHIDAMBARAM, R. — *Bull. Mater. Sci.*, 1984, **6**, 633.

55. MEYERS, M. A. — *Sci Met.*, 1978, **12**, 21.

56. SMITH, C. S. — *Trans AIME*, 1958, **212**, 574.

57. MOGILEVSKY, M. A. — *Shock waves and high strain rate phenomena in metals* (M. A. Meyers and L. E. Murr, eds), p. 531, 1981, Plenum.

58. GILMAN, J. J. — *J. Appl. Phys.*, 1979, **50**, 4059.

59 GODWAL, B. K., NG, A. AND JEANLOZ, R. — *High Pressure Res* , 1992, **10**, 687.

60. GODWAL, B. K., SIKKA, S. K. AND CHIDAMBARAM, R. — *Phys. Rep.*, 1983, **102**, 121.

61. ROSS, M. — *Rep. Prog Phys.*, 1985, **48**, 1.

62. CHIDAMBARAM, R. — *High Pressure Res.*, 1992, **10**, 659.

63. VOHRA, Y. K. AND AKELLA, J — *Phys. Rev. Lett.*, 1991, **67**, 3563.

64. RAO, R. S., GODWAL, B. K. AND SIKKA, S. K. — *Phys. Rev. B*, 1992, **46**, 5780.

65. SHARMA, S. M. AND SIKKA, S. K. — *Prog. Mater Sci* (in press).

66. LYNCH, W. AND DRICKAMER, H. G. — *J Phys. Chem. Solids*, 1965, **26**, 63.

67. SCHULTE, O. NIKOLAENKO, A. AND HOLZAPFEL, W. B — *High Pressure Res.*, 1991, **6**, 169.

68. MEENAKSHI, S., VIJAYAKUMAR, V., GODWAL, B. K. AND SIKKA, S. K. — *Phys. Rev B*, 1992, **46**, 14359.

69. TAKEMURA, K. — *Phys Rev. Lett.*, 1995, **75**, 1807.

70. POTZEL, W *et al* — *Phys. Rev Lett.*, 1995, **74**, 1139.

71. CHRISTY, A. G. — *Acta Cryst. B*, 1993, **49**, 987.

72. GUPTA, S. C. AND CHIDAMBARAM, R. — *High Pressure Res.*, 1994, **12**, 51.

73. SHARMA, S. M., VIJAYAKUMAR, V., SIKKA, S. K. AND CHIDAMBARAM, R. — *Pramana*, 1985, **25**, 75.

74. DEB, S. K. *et al.* — *Phys. Rev. B*, 1993, **47**, 11491.

75. GYANCHANDANI, J. S., GUPTA, S. C., SIKKA, S. K AND CHIDAMBARAM, R. — *High Pressure Res.*, 1990, **4**, 472.

76. SIKKA, S. K. — Recent trends in high pressure research, *Proc. XIII AIRAPT Int. Conf. on High Pressure Science and Technology*, 1992, (A. K. Singh, ed.), Oxford and IBH, New Delhi, p. 254, 1992.

77. HEINE, V. — *Condensed Matter Phys.*, 1994, **16**, 379.

78. PAYNE, M. C., TETER, M. P. AND ALLEN, D. C. — *Rev. Mod. Phys.*, 1992, **64**, 1045.

79. GALLI, G. AND PARRINELLO, M. — *Computer simulations in material science* (M. Meyer and V. Pontikis, eds), p. 257, 1991, Kluwer Academic.

80. GILLAN, M. J. — *Rev. Mod Phys*, 1992, **64**, 257.

81. YIN, M. T. AND COHEN, M. L. — *Phys. Rev. B*, 1982, **26**, 5668.

82. PICKETT, W. E. — *Comput. Phys Rep.*, 1989, **9**, 115.

83. ROSENGAARD, N. M. AND SKRIVER, H. L. — *Phys. Rev*, 1994, **50**, 4848.

84. SANKARAN, H., SHARMA, S. M. AND SIKKA, S. K. — *J Phys.. Condensed Matter*, 1992, **4**, 261.

85. LOUIE, S. G. — In *Electronic structure, dynamics and quantum structural properties of condensed matter* (J. T Devreese and P. V. Camp, eds), p. 335, 1984, Plenum Press.

86. YIN, M. T. AND COHEN, M. L. — *Phys Rev. Lett.*, 1980, **45**, 1004.

87 MORIARTY, J. A. — *Phys. Rev. B*, 1982, **26**, 1754.

88. SINGH, D. AND PAPACONSTANTOPOULOS, D. A. — *Phys Rev B*, 1990, **42**, 8885.

89. SKRIVER, H. L. — *LMTO method*, 1984, Springer.

90. CAR, R. AND PARRINELLO, M. — *Phys Rev Lett*, 1985, **55**, 2471.

91. VOHRA, Y. K., BRISTER, K. E., WEIR, S. J , DUCLOS, S. J. AND RUOFF, A. L. — *Science*, 1986, **231**, 1136

92. MAO, H. K., WU, Y., SHU, J. F , HEMLEY, R. J. AND COX, D. E. — *Solid St Commun*, 1990, **74**, 1027.

93. XIA, H., DUCLOS, S. J., RUOFF, A. L. AND VOHRA, Y. K. — *Phys. Rev. Lett.*, 1990, **64**, 204.

94. DUCLOS, S. J., VOHRA, Y. K. AND RUOFF, A. L. — *Phys Rev. B*, 1990, **41**, 12021.

95. DUCLOS, S. J., VOHRA, Y. K. AND RUOFF, A. L. — *Phys Rev. B*, 1990, **58**, 775.

96. TAKEMURA, K. — *Phys. Rev B*, 1990, **50**, 16238.

97. MEENAKSHI, S., GODWAL, B K., VIJAYAKUMAR, V., RAO, R. S., JAYARAMAN, A. AND SIKKA, S. K. — *Solid St. Phys C*, 1995, **38**, 367.

98. BROWN, J. M. AND MCQUEEN, R. G. — *Geophys Res.*, 1986, **91**, 7485.

99. HIXSON, R. S., BONESS, D. A., SHANER, J. W. AND MORIARTY, J. A. — *Phys. Rev. Lett.*, 1989, **62**, 637.

100. GODWAL, B. K. AND JEANLOZ, R. — *Phys. Rev B*, 1990, **41**, 744.

101. SIKKA, S. K., RAO, R. S. AND GODWAL, B. K. — *High Pressure Res.*, 1992, **10**, 707.

102. YIN, M. T. AND COHEN, M. L. — *Phys. Rev Lett.*, 1980, **45**, 1004.

103. CHANG, K. J. AND COHEN, M L. — *Phys. Rev B*, 1984, **30**, 5376.

104. CHANG, K. J. AND COHEN, M. L. — *Phys. Rev. B*, 1985, **31**, 7819.

105. VOHRA, Y. K., BRISTER, K. E., DESGRENIERS, S. AND RUOFF, A. L. — *Phys. Rev. Lett.*, 1986, **56**, 1944.

106. MCMAHAN, A. K. AND MORIARTY, J. A. — *Phys. Rev. B*, 1983, **27**, 3235.

107.	OLIZNYK, H. AND HOLZAPFEL, W. B.	*Phys. Rev. B*, 1985, **31**, 4682.
108.	LIU, A. Y., GARCIA, A., COHEN, M. L. GODWAL, B. K. AND JEANLOZ, R.	*Phys. Rev. B*, 1991, **43**, 1795.
109.	JOHANSSON, B., AHUJA, R., ERIKSSON, O. AND WILLS, J. M.	*Phys. Rev. Lett.*, 1995, **75**, 280.
110.	RAO, R. S., GODWAL, B. K. AND SIKKA, S. K.	to be communicated to *High Pressure Res.*
111.	MCQUEEN, R. G., MARSH, S. P., TAYLOR, J. W., FRITZ, J. N. AND CARTER, W. J.	In *High velocity impact phenomena* (R. Kinslow, ed.), p. 293, 1971, Academic.
112.	KUTSAR, A. R. AND GERMAN, V. N.	*Proc. 3rd Int. Conf. on Titanium*, Moscow, 1976.
113.	CARTER, W. J.	In *Metallurgical effects of high strain rate* (R. W. Rohde, *et al.*, eds), pp. 171–184, 1973, Plenum.
114.	GUPTA, S. C., DASWANI, J. M., SIKKA, S. K. AND CHIDAMBARAM, R.	*Curr. Sci.*, 1993, **65**, 399.
115.	CHELIKOWSKY, J. R., KING, H. E., TROULLIER, N. JR., MARTINS, J. L. AND GLINNEMANN, J.	*Phys. Rev. Lett.*, 1990, **65**, 3309.
116.	DI POMPONIO, A. AND CONTINENZA, A.	*Phys. Rev. B*, 1993, **48**, 12558.
117.	SOMAYAZULU, M. S., SHARMA, S. M., SIKKA, S. K., GARG, N. AND CHAPLOT, S. L.	In *High pressure science and technology*-1993, (S. C. Schmidt *et al.*, eds), p. 815, 1994, American Institute of Physics.
118.	DHEKNE, P. S., RAMESH, K., RAJESH, K., MAHAJAN, S. M. AND KAURA, H. K.	*Electronics Today*, 1993, **26**, 76.
119.	RAO, R. S., GODWAL, B. K., SIKKA, S. K. AND CHIDAMBARAM, R.	In *Supercomputing for scientific visualization* (S. M. Mahajan, eds), p. 151, 1994, Tata McGraw-Hill.
120	RAO, R. S., GODWAL, B. K., SIKKA, S. K. AND CHIDAMBARAM, R.	*Phys. Rev. B*, 1994, **50**, 15632.
121.	CHIDAMBARAM, R., SANYAL, M. K., RAGHUNATHAN, V. S., NAMBISSAN, P. M. G. AND SEN, P.	*Phys. Rev. B*, 1993, **48**, 3030.
122.	KIRKPATRICK, S., GELATT, G. D. JR AND VECCHI, M. P.	*Science*, 1983, **220**, 671.
123.	JAGADEESH, B. S., RAO, R. S. AND GODWAL, B. K.	In *Supercomputing for scientific visualization* (S. M. Mahajan, eds), p. 165, 1994, Tata McGraw-Hill.
124.	JAGADEESH, B. S., RAO, R. S. AND GODWAL, B. K.	In *High performance computing* (S. Sahni *et al.*, eds), 1996, pp. 175–180, Tata McGraw-Hill.
125.	VANDERBILT, D.	*Phys. Rev. B*, 1990, **41**, 7892.
126.	BLOCHL, P. E. AND PARRINELLO, M.	*Phys. Rev. B*, 1992, **45**, 9413.
127.	SUGINO, O. AND CAR, R.	*Phys. Rev. Lett.*, 1995, **74**, 1823.
128.	WENTZCOVITCH, R. M., ROSS, N. L AND PRICE, G. D.	*Phys. Earth Planet. Interiors*, 1995, **90**, 101.
129.	LUO, H. AND RUOFF, A. L.	*Phys. Rev. B*, 1993, **48**, 569.

130. LANGRETH, D. C. AND MEHL, M. J. *Phys. Rev. Lett.*, 1981, **47**, 446.

131. SVANE, A. AND GUNNARSSON, O. *Phys. Rev. Lett.*, 1990, **65**, 1148.

132. HAMANN, D. R. *Phys. Rev. Lett.*, 1996, **76**, 660.

133. ROSS, M. AND YOUNG, D. A. *A. Rev. Phys. Chem.*, 1993, **44**, 61.

134. SIKKA, S. K., GODWAL, B. K. AND CHIDAMBARAM, R. In *High pressure shock compression of solid* (J. R. Asay and M. Sahinpoor, eds), Springer Verlag (under publication).

135. YOO, C. S., HOLMES, N. C., ROSS, M., WEBB, D. J. AND PIKE, C. *Phys. Rev. Lett.*, 1993, **70**, 3931.